2013 IEEE 10th International Symposium on Biomedical Imaging:
From Nano to Macro
San Francisco, CA, USA, April 7-11, 2013

SPOKE PULSE DESIGN IN MAGNETIC RESONANCE IMAGING USING GREEDY MINIMAX ALGORITHM

Hao Sun[1], *Daniel S.Weller*[1], *Alan Chu*[2], *Sathish Ramani*[1],
Daehyun Yoon[3], *Jon-F. Nielsen*[2], *Jeffrey A. Fessler*[1]

[1]Department of Electrical and Electronic Engineering, University of Michigan-Ann Arbor
[2]Department of Biomedical Engineering, University of Michigan-Ann Arbor
[3]Department of Radiology, Stanford University

ABSTRACT

Spoke RF pulse design in MRI requires joint optimization of the k-space trajectory and RF pulse weights. This design task is often modelled as a sparse approximation problem with a cost function evaluating the l_2 norm of the excitation error, which can be approximately solved using the orthogonal matching pursuit (OMP) algorithm. However, l_2 optimization does not strictly regulate a maximum deviation between excitation and desired patterns, and may leave bright or dark spots in the image. In this paper, we model the pulse design problem as a sparse approximation problem with an l_∞ norm cost function, and propose a greedy algorithm for solving this new problem. Simulation results demonstrate that our algorithm can produce improved spoke RF pulses (reduced maximum error) compared to l_2 optimization.

Index Terms— spoke pulse, OMP , l_∞ norm, minimax, RF shimming

1. INTRODUCTION

The spoke excitation k-space trajectory (also known as echo volumnar or fast kz) has several applications in MRI, such as B1 shimming [1]. A spoke RF pulse consists of a train of short (<1 msec) sinc subpulses. A through-plane gradient is transmitted simultaneously with the RF subpulses to achieve slice selection, and gradient blips in the kx and ky directions are interleaved between subpulses to achieve within-slice modulation. The gradient blips determine the in-plane k-space locations of those subpluses, which is referred to as phase encoding location. In practice, only a small number of subpulses can be transmitted due to time constraints on the whole RF pulse. Therefore, it is desirable to select only a few in-plane phase encoding locations. These locations are not selected a priori but are chosen as part of the spoke pulse design. In other words, the k-space trajectory and RF pulse weights should be designed jointly. This problem can be solved by exhaustively searching all the possible phase encoding locations and selecting the best, but this will lead to a combinatorial problem, which is hard to solve online while the subject is in the scanner. Recently, several approaches using orthogonal matching pursuit (OMP) [2] or modified OMP have been proposed, which achieve good approximations with much less computation time [1, 3–6]. However, all of these approaches attempt to minimize the l_2-norm of excitation error, which does not strictly enforce a maximum deviation (l_∞-norm) between the desired and actual excitation patterns. This can result in undesired image artifacts such as bright or dark spots, which may decrease the diagnostic utility of the image. Therefore, in this paper, we propose to model the spoke pulse design problem as a sparse approximation problem with minimization of the l_∞-norm to potentially reduce these artifacts. We also propose a greedy-like algorithm to solve it.

NIH F32 EB015914; NIH R21EB012674; NIH R01NS58576

2. THEORY

A typical spoke RF pulse design problem is solved as follows:

$$\min_{\mathbf{x}} \|\mathbf{d} - \mathbf{F}\mathbf{x}\|_2, \text{ such that } \|\mathbf{x}\|_0 = k, \tag{1}$$

where $\mathbf{d} \in \mathbb{C}^N$ is the desired excitation pattern, $\mathbf{F} \in \mathbb{C}^{N \times N}$ is the system matrix under the small tip angle approximation [7]. N is number of pixels in desired excitation pattern. In this paper, we ignore B0 inhomogeneity, which is a reasonable approximation to short RF pulse. Under this assumption, $\mathbf{F}$ is a (inverse) discrete Fourier transform matrix multiplied by the coil sensitivity, and $\mathbf{x}$ is a vector of the RF pulse weights to solve for. The l_0-(semi)norm in (1) ensures k-sparsity of $\mathbf{x}$, i.e., the number of "phase encoding" locations (subpulses) is k. This problem can be solved using OMP.

The above modelling does not regulate spikes that can occur in $\mathbf{d} - \mathbf{F}\mathbf{x}$, which may lead to dark or light spot artifacts in the result image, and we therefore propose the following slightly different problem:

$$\min_{\mathbf{x}} \|\mathbf{d} - \mathbf{F}\mathbf{x}\|_\infty, \text{ such that } \|\mathbf{x}\|_0 = k. \tag{2}$$

This problem explicitly minimizes the maximum absolute value of the entries in $\mathbf{d} - \mathbf{F}\mathbf{x}$, so that the previously mentioned artifacts are reduced. Sparsity is again enforced using the l_0-(semi)norm of $\mathbf{x}$.

To solve the problem in (2), we propose the following greedy selection algorithm, Algorithm 1, shown below.

Algorithm 1 Greedy Algorithm.

1: Input: $\mathbf{F}$, $\mathbf{d}$, and k.
2: Output: $\mathbf{x}$
3: Initialize: $\Lambda = \emptyset$
4: **for** $j = 1$ to k **do**
5: $\quad \lambda_j = \arg\min_{l \notin \Lambda} \min_{\tilde{\mathbf{x}}} \|\mathbf{d} - \mathbf{F}(:, l \cup \Lambda)\tilde{\mathbf{x}}\|_\infty$
6: $\quad \Lambda = \Lambda \cup \{\lambda_j\}$
7: **end for**
8: $\mathbf{x} = \arg\min_{\mathbf{x}} \|\mathbf{d} - \mathbf{F}(:, \Lambda)\mathbf{x}\|_\infty$ {Calc coeffs.}

The inputs to Algorithm 1 are the coil-sensitivity modulated inverse DFT matrix $\mathbf{F}$, the desired excitation pattern $\mathbf{d}$, and the desired sparsity level k. The output is a vector of pulse weights $\mathbf{x}$. The set Λ is a set of indices of the atoms in $\mathbf{F}$ that we use to approximate $\mathbf{d}$. In each iteration, the algorithm finds the index l of an atom of $\mathbf{F}$ that results in the minimum possible l_∞-norm approximation (in Line 5). The index is then added to the set Λ, and the pulse weights $\mathbf{x}$ are calculated by minimizing the l_∞-norm in line 8 using the atoms specified by Λ.

Lines 5 and 8 in Algorithm 1 both involve solving the following unconstrained l_∞-norms minimization problem, where $\mathbf{A}$ are the columns of of $\mathbf{F}$ in line 5 of Algorithm 1.

$$\min_{\mathbf{x}} \|\mathbf{d} - \mathbf{A}\mathbf{x}\|_\infty \tag{3}$$

We propose an efficient algorithm to solve this unconstrained l_∞ norm minimization problem, which is described in detail in section 3. However, algorithm 1 can still be slow in practice because of line 5. Almost *every* single column in $\mathbf{F}$ has to be used for solving an unconstrained l_∞ norm minimization problem. A typical target excitation pattern is 64x64 pixels (e.g., slice selective excitation), which results in $\mathbf{F}$ having 4096 columns, and it would be very time consuming to run our unconstrained l_∞ norm minimization 4096 times at each iteration of algorithm 2. It it therefore desirable to use fewer candidate atoms in this step. One way to do this is to try only the q atoms (e.g. $q = 10$) that have the q largest dot products with the residual. This algorithm is shown below as Algorithm 2, and is called "greedy-like" because it is not strictly guaranteed to pick the best l_∞-norm minimization vector at each iteration.

Algorithm 2 Greedy-like Algorithm.

1: Input: $\mathbf{F}$, $\mathbf{d}$, k, and q.
2: Output: $\mathbf{x}$
3: Initialize: $a = 0$, $\Lambda = \emptyset$
4: **for** $j = 1$ to k **do**
5: $\quad \mathbf{r} = \mathbf{d} - \mathbf{a}$ {Update residual.}
6: $\quad p = \mathbf{F}'\mathbf{r}$ {Dot products.}
7: $\quad S = \{$ set of (indices $\notin \Lambda$) of max q elements of p $\}$
8: $\quad \lambda_j = \arg\min_{l \in S} \min_{\tilde{\mathbf{x}}} \|\mathbf{d} - \mathbf{F}(:, l \cup \Lambda)\tilde{\mathbf{x}}\|_\infty$
9: $\quad \Lambda = \Lambda \cup \{\lambda_j\}$
10: $\quad \mathbf{x} = \arg\min_{\mathbf{x}} \|\mathbf{d} - \mathbf{F}(:, \Lambda)\mathbf{x}\|_\infty$ {Calc coeffs.}
11: $\quad \mathbf{a} = \mathbf{F}(:, \Lambda)\mathbf{x}$ {Update approximation.}
12: **end for**

In line 6 of Algorithm 2, the dot product of the residual with each atom in $\mathbf{F}$ is computed. In line 7, indices of the q candidate atoms not in Λ that have the q biggest dot products are saved in the set S. Finally, in line 8, the algorithm picks the atom in S that when added to the set Λ, results in the minimum l_∞-norm approximation to $\mathbf{d}$. The l_∞-norms in lines 8 and 10 are again solved using the proposed unconstrained l_∞ norm minimization algorithm, to be described below.

Algorithm 2 uses the dot products, $\mathbf{F}'\mathbf{r}$, to eliminate the need for trying every atom with the relatively slow procedure of unconstrained l_∞ norm minimization algorithm. This shortcut does not guarantee that the q candidate atoms with largest dot product will generate the lowest l_∞-norm out of all possible atoms. Thus, the choice of q presents a tradeoff between algorithm speed and "greediness."

3. SOLVING THE UNCONSTRAINED L_∞ MINIMIZATION PROBLEM

This section describes our algorithm to solve (3). We propose to use variable-splitting to transform this unconstrained problem into the following equivalent constrained problem:

$$\min_{\mathbf{x},\mathbf{v}} \|\mathbf{v}\|_\infty, \text{ such that } \mathbf{v} = \mathbf{A}\mathbf{x} - \mathbf{d}. \tag{4}$$

Then we form the augmented Lagrangian function:

$$L(\mathbf{x}, \mathbf{v}, \mathbf{y}) = \|\mathbf{v}\|_\infty + \frac{\mu}{2}\|\mathbf{A}\mathbf{x} - \mathbf{v} - \mathbf{d} - \mathbf{y}\|_2^2 \tag{5}$$

where $\mathbf{y}$ is the scaled dual variable and μ is a penalty parameter. We then solve the $\min_{\mathbf{x},\mathbf{v},\mathbf{y}} L(\mathbf{x}, \mathbf{v}, \mathbf{y})$ problem using the following alternating direction method of multipliers (ADMM) update [8]

$$\mathbf{x}^{k+1} = \operatorname{argmin}_{\mathbf{x}} L(\mathbf{x}, \mathbf{v}^k, \mathbf{y}^k) \tag{6}$$

$$\mathbf{v}^{k+1} = \operatorname{argmin}_{\mathbf{x}} L(\mathbf{x}^{k+1}, \mathbf{v}, \mathbf{y}^k) \tag{7}$$

$$\mathbf{y}^{k+1} = \mathbf{y}^k + (\mathbf{A}\mathbf{x}^{k+1} - \mathbf{v}^{k+1} - \mathbf{d}) \tag{8}$$

The update of x is easy, which is $\mathbf{x}^{k+1} = \mathbf{A}^{+}(\mathbf{v}^k + \mathbf{d} + \mathbf{y}^k)$, where $\mathbf{A}^{+}$ is the pseudo-inverse of $\mathbf{A}$. The update of $\mathbf{y}$ is trivial, which consists of adding the primal error to the current $\mathbf{y}$. To solve (7) and update v, we propose the following method. The derivation is similar to the approach for deriving the soft-thresholding method.

Let $\mathbf{c} = \mathbf{A}\mathbf{x}^k - \mathbf{d} - \mathbf{y}^k$, and equation (7) now becomes:

$$\min_{\mathbf{v}}(\|\mathbf{v}\|_\infty + \frac{\mu}{2}\|\mathbf{v} - \mathbf{c}\|_2^2) \tag{9}$$

To solve the problem of this form, we divide it to two steps: first consider minimizing the function $h(\mathbf{v}) = u + \frac{\mu}{2}\|\mathbf{v} - \mathbf{c}\|_2^2$ over complex $\mathbf{v}$ that satisfies $\|\mathbf{v}\|_\infty \leq u$ for fixed u; then minimize this minimum value, which is a function of u, over u. In the first step, the objective $h(\mathbf{v})$ is obviously separable in $\mathbf{v} = [v_1, \ldots, v_M]^T$, so each v_i can be chosen independently. Consider the corresponding element of $\mathbf{c} = [c_1, \ldots, c_M]^T$: if $|c_i| \leq u$, then setting $v_i = c_i$ obviously minimizes $|v_i - c_i|^2$ while satisfying $|v_i| \leq u$. Otherwise, the closest v_i to c_i lies on the boundary $|v_i| = u$, and at the phase closest to c_i: $v_i = c_i \frac{u}{|c_i|}$. Putting these together yields the thresholding-like solution

$$\hat{v}_i(u) = c_i \frac{\min\{u, |c_i|\}}{|c_i|}. \tag{10}$$

Then, if we plug our optimal v_i's into $h(\mathbf{v})$, we get

$$h(\hat{\mathbf{v}}(u)) = u + \frac{\mu}{2}\sum_{i=1}^{M} \max\{|c_i| - u, 0\}^2 \tag{11}$$

Let $\phi_i(u) = \frac{1}{2}\max\{|c_i| - u, 0\}^2$; this function is convex over all u and strictly convex when $u < |c_i|$. Then, re-parameterizing $h(\cdot)$ in terms of distance u yields

$$h(u) = u + \mu\sum_{i=1}^{M} \phi_i(u). \tag{12}$$

Since the sum of convex functions is strictly convex as long as one is strictly convex, we see that $h(u)$ is strictly convex for $u < \|\mathbf{c}\|_\infty$, which is the maximum distance we would consider (since its boundary contains $\mathbf{v} = \mathbf{c}$). The derivative of $\phi_i(u)$ is $\min\{u - |c_i|, 0\}$, so the derivative

$$\dot{h}(u) = 1 + \mu\sum_{i=1}^{M} \min\{u - |c_i|, 0\}. \tag{13}$$

The extremum $u^* \in (0, \|\mathbf{c}\|_\infty)$ must satisfy

$$\frac{1}{\mu} = \sum_{i=1}^{M} \max\{|c_i| - u^*, 0\} = \sum_{i:|c_i|>u^*} (|c_i| - u^*). \tag{14}$$

Finding this extremum is easy: denote $\tilde{\mathbf{c}} = [\tilde{c}_1, \ldots, \tilde{c}_M]^T$ the vector $\mathbf{c}$ sorted by magnitude largest to smallest, and find the largest value of I such that $\sum_{i=1}^{I}(|c_i| - |c_I|) \leq 1/\mu$. Then, u^* lies between $|c_I|$ and $|c_{I+1}|$ (or between $|c_M|$ and zero, for $I = M$); in particular, $u^* = |c_I| - (1/\mu - \sum_{i=1}^{I}(|c_i| - |c_I|))/I$. It is possible if $I = M$ that u^* becomes less than zero for μ is small enough, in which case the optimal $u^* = 0$. Plugging in u^* into Eq. (10) yields the non-iterative solution $\mathbf{v}$ for the sub-problem (9) which is used in the update in (7).

4. SIMULATION RESULTS

The simulation contains two parts. First, we demonstrate that our algorithm can solve the unconstrained l_∞ norm minimization problem shown in equation (3). Second, we simulate our algorithms for the overall l_∞ norm sparse approximation problem defined in equation (2). In the first simulation, we first create a 2D DFT matrix with size n by n and modulate it by the sensitivity map. Then we randomly pick m (=n/2) columns from this matrix to form matrix $\mathbf{A}$ in (3). We randomly create a vector b with length n, and feed them into our code and plot $\|Ax - b\|_\infty$ versus number of iterations, The simulation result is shown in Fig. 1. The coefficient x is initialized by obtaining the least square solution to (3), and μ is set to 2 in (5) for ADMM. As we can see, the cost converges after about 40 iterations. The decrease of the cost function is not monotonic, which is reasonable since the ADMM method does not guarantee monotonic convergence. To test whether it converges to the optimal solution, we used the output of our algorithm as an input to the MATLAB fminsearch function and observed no improvement in the cost function. This suggests that our algorithm finds a local minimum, which should be the global minimum since the cost function is convex.

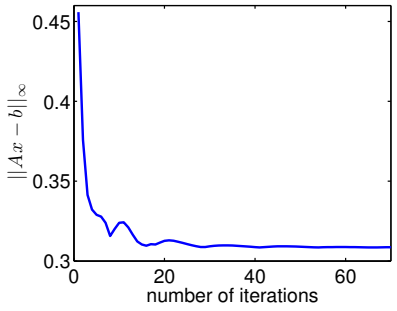

Fig. 1: test of unconstrained l_∞ norm minization

In the second simulation, we investigated our proposed method in the context of RF shimming. RF shimming is an important application of spoke RF pulse design, especially in high field or parallel excitation, with the goal of uniformly exciting a region with non-uniform transmit sensitivities. This problem is typically modelled as a sparse approximation problem as shown in (1). OMP is one conventional algorithm to solve problem (1) and there are many modifications to OMP to improve its performance for RF spoke pulse design [1, 3–6]. In our simulation, we compared our algorithm to a modified OMP with exactly the same structure as our

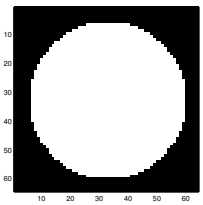

(a) Desired pattern

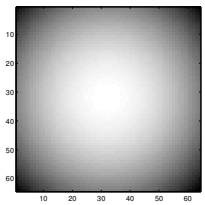

(b) Sensitivity map

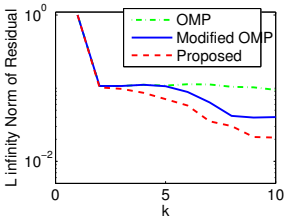

(c) l_∞ norm of residual

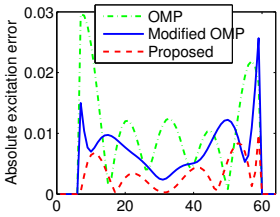

(d) cross line in image

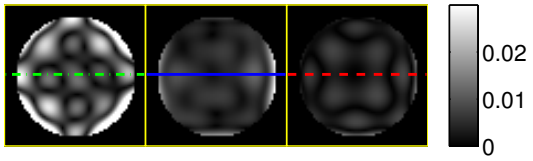

(e) Difference between excitation patterns and desired pattern (left: OMP; middle: modified OMP; right:proposed)

Fig. 2: Comparing OMP and proposed algorithm

proposed Algorithm 2 except that the l_∞ norm minimization of lines 8 and 10 are replaced with l_2 norm minimization. We choose this algorithm for comparison for two reasons: first, keeping the structure the same provides a common ground for the choice of the norm between l_∞ and l_2 norm; second, there are many variations of OMP, and it is not practical to compare all of them. As a reference, we also include the classical OMP in our simulation. In the simulation, the desired excitation pattern is a uniform circle shown in Fig.2-a, which is then reshaped to a column vector $\mathbf{d}$ (4096 by 1). The region outside the circle is not in our region-of-interest. We create the system matrix $\mathbf{F}$ by multiplying a 2D DFT matrix (4096 by 4096) with the nonuniform coil sensitivity map shown in Fig.2-b. The comparison of l_∞ norm versus number of phase encoding locations (k) is shown in Fig. 2-c for OMP, modified OMP and the proposed Algorithm 2. We set our simulation range of k to be 1 to 10 since we usually want a small number of spokes in practice to reduce overall pulse length. We can see in Fig.2-c that OMP fails to significantly decrease the l_∞ norm of the residual after k = 2, while modified OMP can decrease l_∞ norm further, but still has higher (about twice) l_∞ norm compared to our proposed algorithm. The difference between desired and true excitation patterns is shown in Fig.2-e. It demonstrates that the excitation pattern of our proposed algorithm is much closer to the desired pattern than the OMP algorithm and modified OMP algorithm. We also plot the cross section line of excitation error for all three methods in Fig. 2-d, and the proposed method has the smallest ripples.

5. CONCLUSION

In this paper, we proposed a novel method to model the spoke RF pulse design problem in MRI: instead of modelling it as a sparse approximation problem with a l_2 norm cost function, we use l_∞ in the cost function to limit the maximum error. To solve this new problem, we proposed a greedy algorithm. The core part of that greedy algorithm is an unconstrained l_∞ norm minimization in the complex domain (3), and that is solved using variable-splitting and ADMM. An non iterative solution is derived to solve the most difficult part in the ADMM update (9) efficiently. To our knowledge, this is also novel. Our simulation results show that our proposed model and algorithm result in a much smaller maximum error than the classical OMP and the modified OMP (i.e., the l_2 norm counterpart of proposed algorithm) for the spoke RF pulse design problem. Experimental validation will be conducted in the near future. We plan to extend our proposed method by including the B0 imhomogeneity effect and considering parallel excitation. Also, for some applications that only the magnitude of excitation pattern is of interest, we may modify our method to solve a "magnitude minimax" problem and compare it with the "magnitude least square" formulation [9].

6. REFERENCES

[1] W. A. Grissom, M-M. Khalighi, L. I. Sacolick, B. K. Rutt, and M. W. Vogel, "Small-tip-angle spokes pulse design using interleaved greedy and local optimization methods," *Mag. Res. Med.*, 2012.

[2] J. A. Tropp, "Algorithms for simultaneous sparse approximation, Part II: convex relaxation," *Signal Processing*, vol. 86, no. 3, pp. 589–602, Mar. 2006.

[3] C. Ma, D. Xu, K. F. King, and Z. P. Liang, "Joint design of spoke trajectories and RF pulses for parallel excitation," *Mag. Res. Med.*, vol. 65, no. 4, pp. 973–85, Apr. 2011.

[4] D. Yoon, J. A. Fessler, A. G. Gilbert, and D. C. Noll, "Fast joint design method for parallel excitation RF pulse and gradient waveforms considering off-resonance," *Mag. Res. Med.*, vol. 68, no. 1, pp. 278–85, July 2012.

[5] D. Chen, F. Bornemann, M. Vogel, L. Sacolick, G. Kudielka, and Y. Zhu, "Sparse parallel transmit pulse design using orthogonal matching pursuit method," in *Proc. Intl. Soc. Mag. Res. Med.*, 2009, p. 171.

[6] A. C. Zelinski, L. L. Wald, K. Setsompop, V. K. Goyal, and E. Adalsteinsson, "Sparsity-enforced slice-selective MRI RF excitation pulse design," *IEEE Trans. Med. Imag.*, vol. 27, no. 9, pp. 1213–29, Sept. 2008.

[7] J. Pauly, D. Nishimura, and A. Macovski, "A k-space analysis of small-tip-angle excitation," *J. Mag. Res.*, vol. 81, no. 1, pp. 43–56, Jan. 1989.

[8] S. Boyd, N. Parikh, E. Chu, B. Peleato, and J. Eckstein, "Distributed optimization and statistical learning via the alternating direction method of multipliers," *Found. & Trends in Machine Learning*, vol. 3, no. 1, pp. 1–122, 2010.

[9] K. Setsompop, L. L. Wald, V. Alagappan, B. A. Gagoski, and E. Adalsteinsson, "Magnitude least squares optimization for parallel radio frequency excitation design demonstrated at 7 Tesla with eight channels," *Mag. Res. Med.*, vol. 59, no. 4, pp. 908–15, Apr. 2008.